Electronic Supplementary Material (ESI) for Physical Chemistry Chemical Physics.

Theoretical approaches to defect mechanisms and transport properties of compounds used for electrode and solid-state electrolyte in alkali-ion batteries

Yohandys A. Zulueta[a] and Minh Tho Nguyen[b,c*]

[a] *Departamento de Física, Facultad de Ciencias Naturales y Exactas, Universidad de Oriente, CP- 90500, Santiago de Cuba, Cuba. Email:* yzulueta@uo.edu.cu

[b] *Laboratory for Chemical Computation and Modeling, Institute for Computational Science and Artificial Intelligence, Van Lang University, Ho Chi Minh City, Vietnam.*

[c] *Faculty of Applied Technology, School of Technology, Van Lang University, Ho Chi Minh City, Vietnam*

* Corresponding author; Email: minhtho.nguyen@vlu.edu.vn

Supplementary Information (SI)

1 Computational protocols to disclose relevant properties of battery materials

1.1 DFT protocol

The purpose of this supplementary information is to disseminate a practical protocol disclosing the main ground state properties of known or hypothetical battery materials. Such a theoretical protocol using density functional theory (DFT) can be used for a number of purposes:

1. Determination and prediction of lattice parameters and electronic structure properties (such as energy gap), density of the states and projected density of the states to disclose the bonding nature of the constituent ions and their contribution to the electronic properties.
2. Exploration of first-order thermodynamic stability of the compounds considered such as the standard molar and standard formation enthalpies;

3. Exploration of second-order thermodynamic stability such as the stability upon individual constituent ion during the insertion/disinsertion process, with particular interest on alkali ions; and
4. Exploration of open cell voltage and, if it is possible, theoretical capacity.

The open cell voltage (V) can also be obtained from DFT computations. The open cell voltage is directly proportional to the alkali chemical potential difference between cathode ($\mu_{A^+}^{cathode}$) and anode ($\mu_{A^+}^{anode}$):[1-3]

$$V = -\left(\mu_{A^+}^{cathode} - \mu_{A^+}^{anode}\right)/\Delta x F \quad (1)$$

where F is the Faraday constant and Δx is the charge displaced from the electrode considered. Equation (1) can be simplified in terms of Gibbs free energy and further in total energy.[1-3]

1.2 Molecular dynamics simulations

Molecular dynamics (MD) is well-known as a powerful simulation tool that permits the motion of the particles in a system to be directly studied.[4,5] This methodology is based on the numerical solution of the second Newton law of motion for a particle (ions, atoms) system. For instance, MD uses the interatomic potentials (force fields) to evaluate the interatomic interactions explicitly. When it is enabled for DFT computations, *ab initio* molecular dynamics emerge in which the interatomic interactions are evaluated from pseudopotentials instead of a classical force field. Further details concerning the MD backgrounds can be found elsewhere.

The mean-square displacement (MSD) at each temperature (T) of the ion considered is calculated by the equation (2):

$$MSD(t) = \frac{1}{N}\sum_{i=1}^{N}\left\langle\left[r_i(t_0 + t) - r_i(t_0)\right]\right\rangle^2 \quad (2)$$

where N is the number of mobile species, t_0 the required time for the simulation box reaches the thermodynamics equilibrium (equilibrium time) and r_i the atomic coordinates of the mobile species considered in the simulation box. The plot of MSD at a temperature T, against simulation time t, must be a straight line, and the slope of this line represents the diffusion coefficient D as expressed in equation (3):

$$MSD = 2dDt \tag{3}$$

where d is the degree of freedom.[4,5]

The ionic conductivity or direct current conductivity (σ_{DC}) can be obtained employing the Nernst–Einstein relation (4):

$$\sigma_{DC}(T) = H_V N q^2 D(T)/k_B T \tag{4}$$

where q is the charge of the mobile ion, N represents the number of mobile ions per unit volume, k_B the Boltzmann constant, and H_V represents the Haven's ratio.[3,6]

After application of this procedure for various temperature values, we obtain a series of values for $D(T)$ and $\sigma_{DC}(T)$, that can be fitted with the aid of an Arrhenius-type function :

$$D(T) = D_0 exp(-Ea/k_B T) \; ; \; \sigma_{DC}(T) = \sigma_0 exp(-Ea/k_B T) \tag{5}$$

to obtain the simulated activation energies (Ea) for diffusion and electrical conduction, respectively. In equation (5), D_0 and σ_0 are pre-exponential factors for diffusion and conduction, respectively. The simulated values of $D(T)$ and in particular of $\sigma_{DC}(T)$ are valuable parameters as they can be directly compared to the experimental results reported in the literature. This provides a certain calibration for the computational results.[43-45]

1.3 Static simulations

1.3.1 Nudged elastic band.

Another popular method to explore transport properties of compounds is the nudged elastic band (NEB) method.[8,9] NEB can be regarded as derived from the classical transition state theory (TST) of chemical kinetics. The TST is indeed crucial in the understanding and design of chemical reaction, alkali migration path, and activation energy involved in battery materials.[8,9] This method considers two main data, namely the true transition state structure and the minimum energy migration path, including the activation energy by taking a hypothetical reaction path. The synchronous transit method (Sync) is efficient to predict the transition state structure, whereas the NEB discloses the minimum energy path, the activation energy, and together with the TST, the diffusion coefficient at ambient temperature of the migrating ion considered.[8-10]

The NEB algorithm is in fact a method for constructing a minimum energy pathway between the reactant(s) and product(s) (see Fig. S1). NEB calculations assumes the existence of a sequence of structures (also called images, replicas or reaction coordinates) describing the reaction path. Between initial and final configuration, various intermediate images can be provided intentionally, in which the image interpolation is performed between the reactant and the nearest image, and then between consecutive intermediate replicas until the final configuration. Each NEB optimization cycle consists of energy and gradient evaluations of images with geometries describing the path between the two endpoints (reactant and product). The simplest idea to find the minimum energy path is introducing an interaction between neighboring replicas by a spring with spring constant k.[8-10]

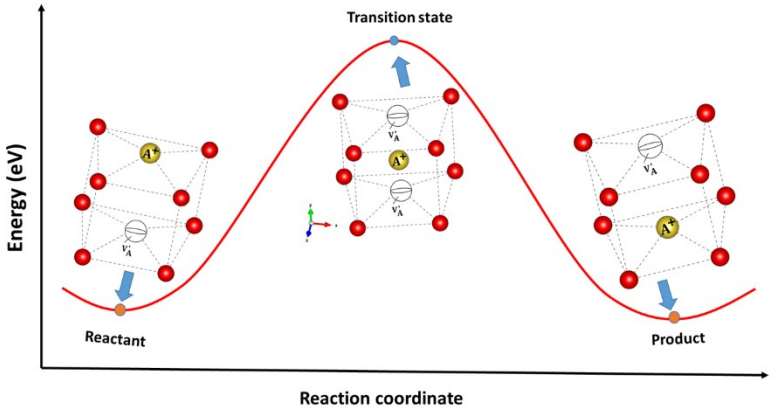

Figure S1: Scheme representing a hypothetical reaction pathway including the reactant(s), transition state and product(s).

The activation energy is obtained from the energy difference between reactant(s) and transition state. The reaction coordinate corresponding to the energy saddle point discloses the transition state structure (see Fig. S1). The rate constant (Rc) of the hypothetical reaction obeys the Arrhenius-type equation:

$$Rc = \nu exp(-E_a/k_BT) \tag{6}$$

where ν is a constant, E_a the activation energy, k_B the Boltzmann constant and T the temperature.[11] The diffusion coefficient (D) can be evaluated by a similar Arrhenius-type dependence:

$$D = \frac{1}{2}\alpha^2 \nu exp(-E_a/k_BT) = \frac{1}{2}\alpha^2 Rc \tag{7}$$

where α is the diffusion length (or jump distance) of the diffusing ion, ν the attempt frequency (or hopping rate) which amounts to 10^{13} Hz at 25°C.[11]

As the NEB approach implies geometry optimization calculations, the search for transition states can be performed by using either force field or DFT methods.[7,11] Note that, NEB and Sync computations are classified as static simulations, i.e.: the influence of the temperature is

not considered. In this sense, NEB and Sync computations are good for a rapid predictions of transport properties and diffusion path, but large-scale MD simulations is advisable to include the influence of other factors, including the temperature. Another consideration for these static simulations is the selection of the force field. In some cases, the replica number (or reaction coordinates) is fundamental, because if a few number of N is selected, the real transition state structure can be hidden between reaction coordinates. The spring constant, *k*, connecting the replicas, is other factor to be considered. There are two variants for selecting *k*: it can be fixed or varying between replica in a value range.[9,10] The reader can guess the optimum *k* value to ensure rapid convergence for the computations.

1.3.2 Defects energetics

Defect energetics protocol has abundantly been described elsewhere.[12-18] This methodology leads to a determination of the defect -or defect cluster- behavior and their interaction with the local environment in the lattice structure of solid-state materials. This procedure is based on the concept of punctual defects, mainly divided by substitution, interstitial and vacancy. These defects can be present in the lattice structure intentionally, called doping, or accidentally during a sample preparation. A vacancy is generated by a breaking of bonds and results in a structure where the usually occupied lattice sites become unoccupied, which affects the local environment in the crystallographic position where it is created. Interstitial defect is generated when a host or foreign ion occupies empty spaces within the local lattice structure, and it could be created by doping (adding foreigner ions) or interpreted as a consequence of synthesis process. There are semi-chemical equations which describe the appropriate mode of the dopant incorporation into the lattice structure, depending of the stoichiometry of the crystal structure of interest. These equations are called incorporation mechanisms of the dopant. The well-established Kröger-Vink notation is used to describe explicitly the incorporation mechanisms.[19] The Kröger-Vink notation uses three labels to define the defect type. For

instance, considering the ABC lattice structure, if A^{α} and B^{β} are the A substitution positions with a formal ion charge α, and the B host cation with a charge β in the lattice structure, then A_A represents that the ion A is maintained in its crystallographic position in the lattice structure; A_B^c represents the substitution of A^{α} in the crystallographic position of B^{β} and c is the formal charge difference between A and B ions (or net charge), which takes single point (•) and (/) for positive or negative charges, respectively. If $c = 0$ (i.e.; isovalent substitution) a superscript (×) is used; to represent a vacancy of B^{β}, the notation of V_B^{β} is used and the vacancy charge is opposed to the formal charge of the ion considered. Interstitial defect type is represented as A_i^{α}, where the subscript i means interstitial incorporation. When various defect types lie in a crystal structure, the can form a defects cluster. It is important to highlight that the defective lattice structure must be charge compensated to ensure the stability and the proper existence of the compound. The common methodology used to study the defects energetics is based on the Mott-Littleton method (also called two-region or multi-regions strategy), where the defects (isolated defect or defects cluster) are simulated at the infinitely dilute limit.[20] A diagrammatic representation of the Mott-Littleton approximation is shown in Fig. S2. Under this approach, the overall focus where the defects are located is divided in two concentrically spherical regions with radius R1 and R2, respectively. The defect(s) are located in the inner region are referred to as R1, where the atomic interactions are calculated explicitly considering the Coulombic interactions, and the force field. The outer region is treated as a dielectric continuum method. The total defect energy, E_T, is described by equation (8):

$$E_T = E_1(x) + E_{12}(x,\epsilon) + E_2(\epsilon) \quad (8)$$

where the interatomic displacements in the inner region are denoted by x and the external by ϵ, E_1 and E_2 represent the energies of regions 1 and 2, respectively, and E_{12} is the interchange energy between them.

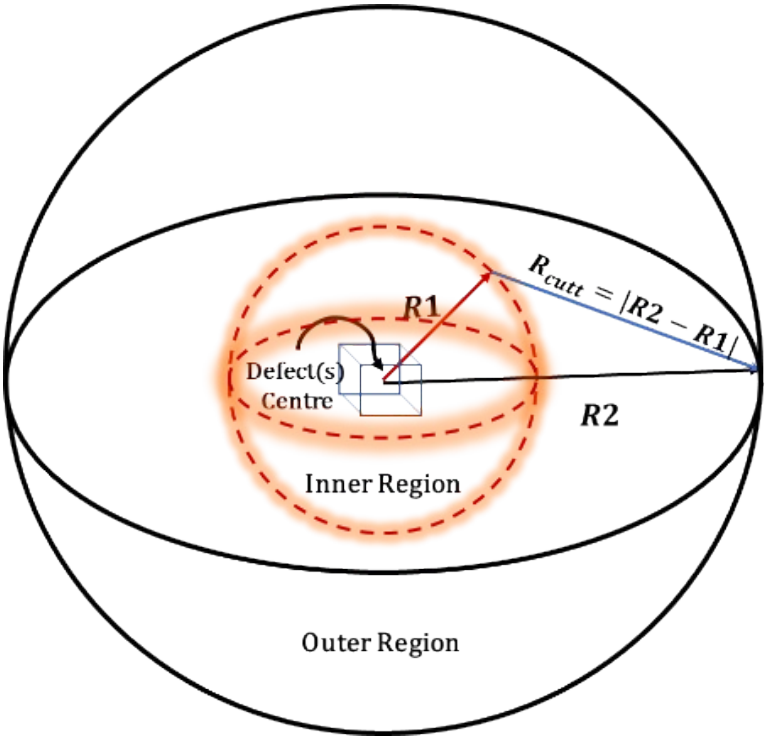

Figure S2: Schematic representation of the two-region strategy.

The procedure to make a defect energetics calculation is standard. A representative example is exposed above concerning defect energetics computation of rare-earth (RE^{3+}) and divalent (M^{2+}) dopants in a hypothetical ABO_3 structure: starting with the unit cell of the subject structure (e.g. ABO_3) by using the two regions strategy calculations, in order to obtain:

1. The RE^{3+} or M^{2+} substitution energy in A^{2+} and B^{4+} into the ABO_3 lattice structure, including the lattice (cohesive) energy of AO, BO_2, RE_2O_3 (or MO_2) and ABO_3 structures.
2. The vacancy formation energy of the host species of ABO_3, i.e.; the required energy to form a A, B and O vacancy.
3. Selection of the incorporation mechanism for the selected dopant.
4. According to the selected dopant and incorporation mechanism, calculation of the solution energy to form all the defects present in the incorporation scheme, i.e.; $RE_{Ti}^{'}, RE_{A}^{\cdot}, M_{A}^{\times}, M_{B}^{''}, V_{O}^{\cdot\cdot}, V_{A}^{''}$ etc., with reference to the Athkar *et. al.* method.[19-21]

5. The binding energy of the defects cluster formed in the considered incorporation scheme is defined as follow:

$$E_{bind} = E_{clus} - \Sigma E_{ins} \quad (9)$$

where E_{bind}, E_{clus} and E_{ins} are the binding, cluster and isolated defect energies, respectively.

6. The final solution energy, as a correction of the solution energy by the binding energy multiplied by a factor depending of the incorporation mechanism considered.

Supplementary Tables and Figures

Table S1: Reaction energy (ΔE in eV/atom) of $A_2B_6X_{13}$ structures in exchange reactions.

$Li_2Sn_6S_{13}$		**A^+**	**Sn^{4+}**	**X^{2-}**
		$LiSn_6S_{13}$	**$Li_2Sn_5S_{13}$**	**$Li_2Sn_6S_{12}$**
	ΔE	8.1	31.9	81.2
$Na_2Sn_6S_{13}$		**A^+**	**Sn^{4+}**	**X^{2-}**
		$NaSn_6S_{13}$	**$Na_2Sn_5S_{13}$**	**$Na_2Sn_6S_{12}$**
	ΔE	7.7	31.9	81.2
$K_2Sn_6S_{13}$		**A^+**	**Sn^{4+}**	**X^{2-}**
		KSn_6S_{13}	**$K_2Sn_5S_{13}$**	**$K_2Sn_6S_{12}$**
	ΔE	7.5	31.9	81.2
$Li_2Ti_6S_{13}$		**A^+**	**Ti^{4+}**	**X^{2-}**
		$LiTi_6S_{13}$	**$Li_2Ti_5S_{13}$**	**$Li_2Ti_6S_{12}$**
	ΔE	8.3	32.9	83.2
$Na_2Ti_6S_{13}$		**A^+**	**Ti^{4+}**	**X^{2-}**
		$NaTi_6S_{13}$	**$Na_2Ti_5S_{13}$**	**$Na_2Ti_6S_{12}$**
	ΔE	8.3	33.0	81.3
$K_2Ti_6S_{13}$		**A^+**	**Ti^{4+}**	**X^{2-}**
		KTi_6S_{13}	**$K_2Ti_5S_{13}$**	**$K_2Ti_6S_{12}$**
	ΔE	7.7	33.0	81.3
$Li_2Ti_6O_{13}$		**A^+**	**Ti^{4+}**	**X^{2-}**
		$LiTi_6O_{13}$	**$Li_2Ti_5O_{13}$**	**$Li_2Ti_6O_{12}$**
	ΔE	6.9	34.3	45.9
$Li_2Sn_6O_{13}$		**A^+**	**Sn^{4+}**	**X^{2-}**
		$LiSn_6O_{13}$	**$Li_2Sn_5O_{13}$**	**$Li_2Sn_6O_{12}$**
	ΔE	6.4	33.6	45.4
$Na_2Sn_6O_{13}$		**A^+**	**Sn^{4+}**	**X^{2-}**
		$NaSn_6O_{13}$	**$Na_2Sn_5O_{13}$**	**$Na_2Sn_6O_{12}$**
	ΔE	9.2	32.8	45.6
$K_2Sn_6O_{13}$		**A^+**	**Sn^{4+}**	**X^{2-}**
		KSn_6O_{13}	**$K_2Sn_5O_{13}$**	**$K_2Sn_6O_{12}$**
	ΔE	8.6	32.9	45.6

Table S2: Thermodynamic data of the $A_2B_6X_{13}$ compounds and their binary decomposition. Band gap (Eg) and open cell voltage (V) are included for comparison [21,22].

Compound	$\Delta_f H_m$ (kJ.mol^{-1})	$\Delta_f H_m$ (kJ.mol^{-1})	Eg (eV)	V (V per A^+/A)
Li_2O	-599	-	-	-
Li_2S	-441	-	-	-
Na_2O	-414	-	-	-
Na_2S	-364	-	-	-
K_2O	-362	-	-	-
K_2S	-406	-	-	-
SnO_2	-581	-	-	-
SnS_2	-152	-	-	-
TiO_2	-944	-	-	-
TiS_2	-410	-	-	-
$Li_2Sn_6O_{13}$	-	-5553	3.03	1.60
$Li_2Sn_6S_{13}$	-	-9618	0.69	2.01
$Na_2Sn_6O_{13}$	-	-5101	2.61	2.30
$Na_2Sn_6S_{13}$	-	-9226	0.57	1.93
$K_2Sn_6O_{13}$	-	-5818	3.08	2.15
$K_2Sn_6S_{13}$	-	-9937	0.49	1.87
$Li_2Ti_6O_{13}$	-	-6740	3.15	1.72
$Li_2Ti_6S_{13}$	-	-8743	0.05	2.09
$Na_2Ti_6O_{13}$	-	-6278	3.5	1.3
$Na_2Ti_6S_{13}$	-	-8390	0.46	2.07
$K_2Ti_6O_{13}$	-	-6035	3.3	1.5-1.7
$K_2Ti_6S_{13}$	-	-8387	0.0	1.93

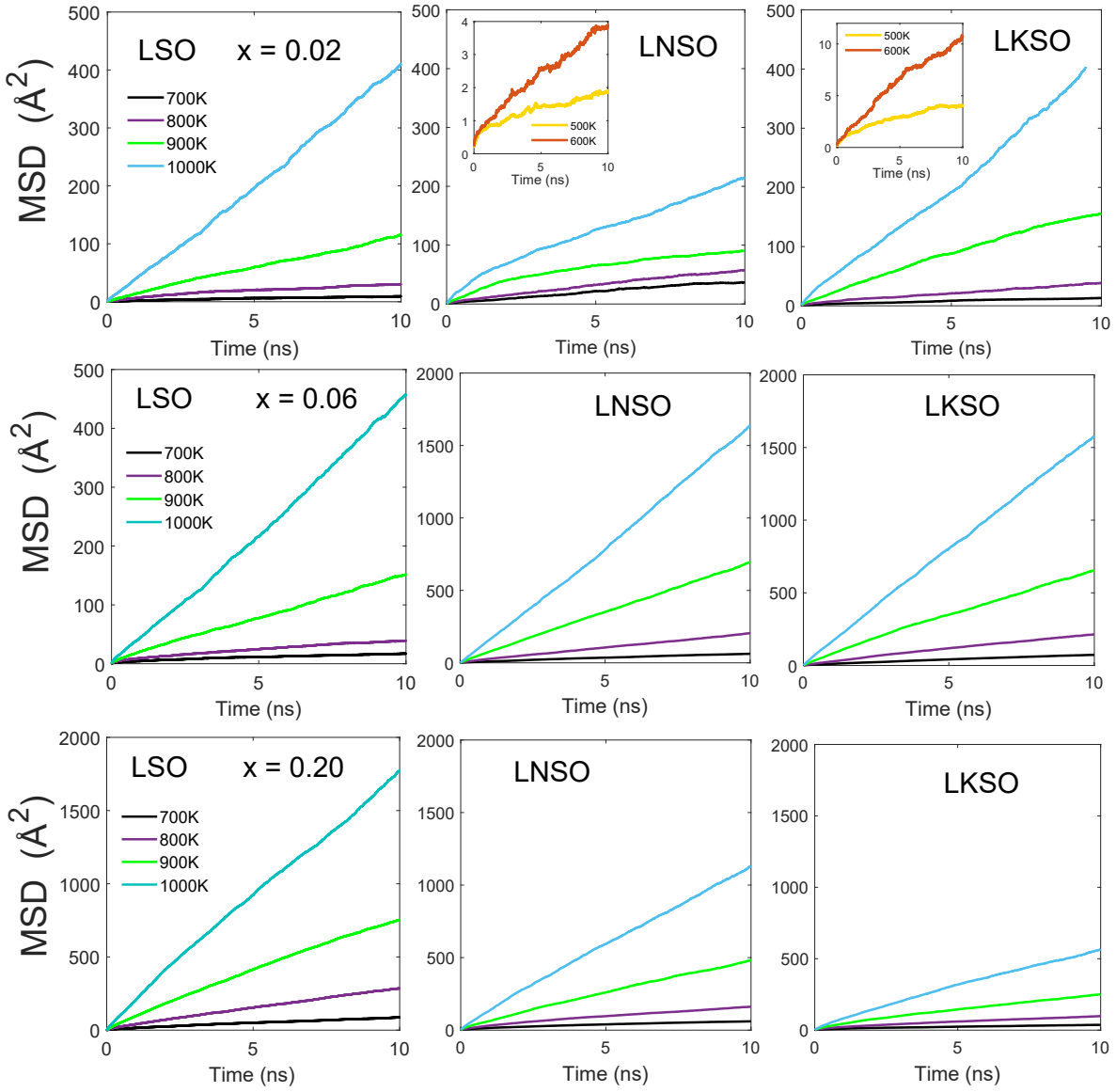

Figure S3. Mean square displacement (MSD) of Li ions in $Li_{2-x}SiO_{3-0.5x}$ (LSO), $Li_{2-x}Na_xSiO_{3-0.5x}$ (LNSO) and $Li_{2-x}K_xSiO_{3-0.5x}$ (LKSO) as a function of dopant concentration (x). Reproduced with permission from reference 5.

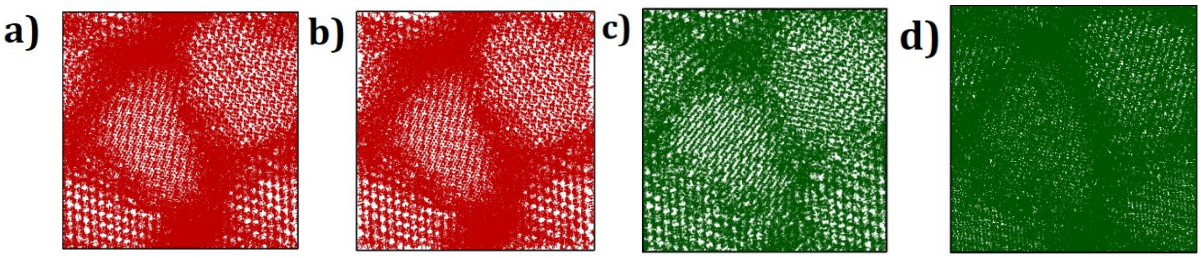

Figure S4. Trajectory density map of a) Li_3OCl, b) Li_3OBr, c) Na_3OCl and d) Na_3OBr compounds after 2ns at 700 K. Red and green lines represents the Li and Na trajectory lines, respectively.

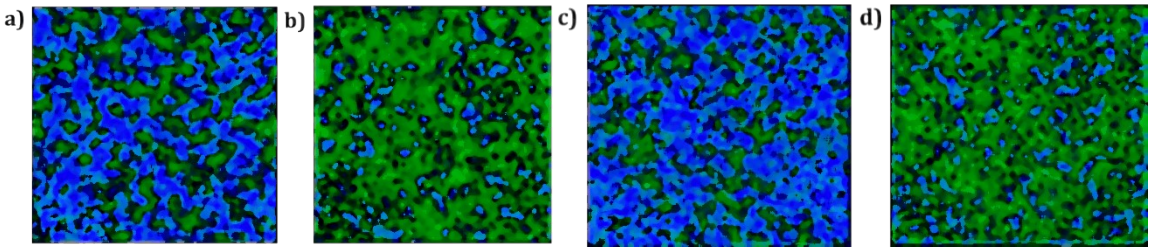

Figure S5. Trajectory plots of Li and Na in a) Li_2NaOCl, b) Na_2LiOCl, c) Li_2NaOBr and d) Na_2LiOBr compounds after 2ns at 700 K. Blue and green color represent the Li and Na trajectory lines, respectively.

References

(1) Zulueta Leyva, Y. A.; Nguyen, M. T. Implications of Oxygen–Sulfur Exchange on Structural, Electronic Properties, and Stability of Alkali-Metal Hexatitanates. *Phys. Status Solidi B.* **2019**, *256* (8), 1800568.

(2) Zulueta, Y. A.; Geerlings, P.; Tielens, F.; Nguyen, M. T. Influence of Oxygen-Sulfur Exchange on the Structural, Electronic, and Stability Properties of Alkali Hexastannates. *J. Phys. Chem. C.* **2019**, *123* (40), 24375–24382.

(3) Nguyen, T. D. H.; Pham, H. D.; Lin, S. Y.; Lin, M. F. Featured Properties of Li^+-Based Battery Anode: $Li_4Ti_5O_{12}$. *RSC Adv.* **2020**, *10* (24), 14071–14079.

(4) Urban, A.; Seo, D. H.; Ceder, G. Computational Understanding of Li-Ion Batteries. *npj Comput. Mater.* **2016**, *2* (1), 1–13.

(5) Rapaport, D. C. The Art Of Molecular Dynamics Simulation, 2nd Ed, Cambridge University Press 1995, Dennis Rapaport, (2004).

(6) Zulueta, Y. A.; Nguyen, M. T. Enhanced Li-Ion Transport in Divalent Metal-Doped Li_2SnO_3. *Dalt. Trans.* **2021**, *50* (8), 3020–3026.

(7) Marx, D.; Hutter, J. Ab Initio Molecular Dynamics: Basic Theory and Advanced Methods, Cambridge University Press, Cambridge, (2009).

(8) Henkelman, G.; Uberuaga, B. P.; Jonsson, H. A. Climbing Image Nudged Elastic Band Method for Finding Saddle Points and Minimum Energy Paths. *J. Chem. Phys*. **2000**, *113*, 9901−9904.

(9) Behn, A.; Zimmerman, P. M.; Bell, A. T.; Head-Gordon, M. Efficient Exploration of Reaction Paths via a Freezing String Method. *J. Chem. Phys.* **2011**, *135* (22), 224108.

(10) Gale, J. D.; Rohl, A. L. The General Utility Lattice Program (GULP). *Mol. Simul.* **2003**, *29*, 291−341.

(11) He, Q.; Yu, B.; Li, Z.; Zhao, Y. Density Functional Theory for Battery Materials. *Energy and Environmental Materials*. **2019**, *2(*4), 264–279.

(12) Behn, A.; Zimmerman, P. M.; Bell, A. T.; Head-Gordon, M. Efficient Exploration of Reaction Paths via a Freezing String Method. *J. Chem. Phys.* **2011**, *135* (22), 224108.

(13) Freeman, C. L.; Dawson, J. A.; Chen, H.; Ben, L.; Harding, J. H.; Morrison, F. D.; Sinclair, D. C.; West, A. R. Energetics of Donor- Doping, Metal Vacancies, and Oxygen-Loss in A-Site Rare-Earth- Doped $BaTiO_3$. A*dv. Funct. Mater.* **2013**, *23*, 3925−3928.

(14) Zulueta, Y. A.; Nguyen, M. T.; Dawson, J. A. Na- And K-Doped Li_2SiO_3 as an Alternative Solid Electrolyte for Solid-State Lithium Batteries. *J. Phys. Chem. C.* **2020**, *124* (9), 4982–4988.

(15) Zulueta, Y. A.; Nguyen, M. T.; Dawson, J. A. Boosting Li-Ion Transport in Transition-Metal-Doped Li_2SnO_3. *Inorg. Chem.* **2020**, *59* (16), 11841–11846.

(16) Zulueta, Y. A.; Nguyen, M. T. Enhanced Li-Ion Transport in Divalent Metal-Doped Li_2SnO_3. *Dalt. Trans.* **2021**, *50* (8), 3020–3026.

(17) Zulueta, Y. A.; Mut, R.; Kaya, S.; Dawson, J. A.; Nguyen, M. T. Strontium Stannate as an Alternative Anode Material for Li-Ion Batteries. *J. Phys. Chem. C* **2021**, *125* (27), 14947–14956.

(18) Zulueta, Y. A.; Nguyen, M. T.; Pham-Ho, M. P. Strontium Stannate as an Alternative Anode for Na- and K-Ion Batteries: A Theoretical Study. *J. Phys. Chem. Solids* **2022**, *162*, 110505.

(19) Kröger, F. A. The Chemistry of Imperfect Crystals, North-Holland Pub. Co. (1964).

(20) Mott, N. F.; Littleton, M. J. Conduction in Polar Crystals. I. Electrolytic Conduction in Solid Salts. *Trans. Faraday Soc*. **1938**, *34*, 485−499.

(21) Akhtar, M. J.; Akhtar, Z. -U -N; Jackson, R. A.; Catlow, C. R. A. Computer Simulation Studies of Strontium Titanate. *J. Am. Ceram. Soc.* **1995**, *78* (2), 421–428.